SF_5-Terminated Fluorinated Schiff Base Liquid Crystals

Jeremy A. Smith,[†] Robert A. DiStasio Jr.,[†,‡] Nicole A. Hannah,[†] Rolf W. Winter,[†] Timothy J. R. Weakley,[⊥] Gary L. Gard,[†] and Shankar B. Rananavare*[,†,§]

Department of Chemistry, Portland State University, 1719 SW 10th Ave., Room 238C, Portland, Oregon 97207; Department of Electrical and Computer Engineering, OGI School of Science and Technology at Oregon Health & Science University, 20000 NW Walker Road, Beaverton, Oregon 97006; and Department of Chemistry, University of Oregon, 1253 University of Oregon, Eugene, Oregon 97403

Received: May 25, 2004; In Final Form: October 12, 2004

Novel liquid crystals based on fluorinated carbon chains and terminated with SF_5 groups are presented for the first time. Attachment of an SF_5 group separated from a benzylidine group by a fluorinated spacer leads to monotropic nematic and smectic phases, while an enantiotropic nematic phase is observed in mixtures. The phase sequence of these new compounds is comparable to hydrocarbon analogues of *n*O.*m* (*n*-alkoxy-*m*-alkylbenzylidine) series. Despite a long alkoxy chain, the nematic → smectic A transition is closer to second order, with $M_{TCP}^{predicted} \approx 0.995$ values that are even higher than for the *n*CB (*n*-alkylcyanobiphenyls) series. Single crystal and quantum computational studies suggest that electrostatic interactions play a major role in governing the value of M_{TCP}. Molecular packing in the crystal structure exhibits monoclinic $P2_1/a$ symmetry. A flexible synthetic strategy that allows the synthesis of another homologous series with a bend in the molecular structure is also presented. The bent core structure of 10O.2 SF_5 investigated shows a monotropic, tilted smectic phase for the higher C_{10} alkoxy chain. The compounds in this series reveal a high degree of undercooling (well above 50 °C), which is rationalized using finite size effects on nucleation.

Introduction

Use of liquid crystals in active-matrix display devices has continued to lead to significant synthetic advances in their material design.[1] The primary driving force for these activities is to design materials that have wide temperature stability, low viscosity, electrical conductivity, and high dielectric anisotropy (optical birefringence) in order to improve display-device performance. Recently, the focus has been directed toward the development of fluorinated liquid crystals[2] because of their desirable wetting properties; these properties are enhanced with the use of fluorinated polyamides (surface alignment layers). Fluorinated liquid crystals are expected to have low rotational viscosities. Several useful reviews have appeared, emphasizing the importance of the location of fluorine groups in the mesogenic structure.[3,4] Selective enhancement of smectic phases is noted when perfluorinated hydrocarbon chains are employed.[5]

To realize high dielectric anisotropy, significant and large longitudinal dipole moments are necessary, and they can be introduced on the long axis of the mesogen by polar functional groups such as F, CN, and NO_2. There have been relatively few studies dedicated to enhancing the polarizability and dipole moments of liquid crystals using the hypervalent SF_5 group.[6] The known mesogens incorporating SF_5 groups attached to the rigid core of liquid crystals exhibit rotational viscosities that are higher than the corresponding cyanobiphenyl (CB) analogues. The nematic liquid crystal phase occurs well above room temperature. To improve the range of accessible liquid crystal phases, we have incorporated an SF_5 moiety along with a perfluorinated aliphatic chain in the classic *n*-alkoxy-*m*-alkylbenzylidine (*n*O.*m*) liquid crystalline homologous series, which displays a range of nematic and smectic phases.[7] Smectic phases exhibited are typically of the monolayer type, so it was interesting to probe whether a terminal strongly polar group would lead to bilayer-type smectics. An additional motivation for introducing a large dipole moment along the longitudinal axis of these molecules was to examine the possibility of generating frustrated smectics as predicted by Prost[8] and observed by Levelut[9] and Kortran et al.[10]

To reduce the rotational viscosities of the SF_5-based compounds, we have selected a fluorocarbon spacer to separate the SF_5 group from the aromatic ring structure. In this paper, we present the synthesis and preliminary characterization of these *n*O.*m* analogues, wherein only the alkyl chains are perfluorinated. Furthermore, an introduction of a $SF_5-CF_2-CF_2$ perfluorinated group provides the distinct possibility of microscopic phase separation with the fluorinated chains separated from the hydrocarbon chains. Such demixing phenomena are well-known in hydrocarbon/fluorocarbon mixtures in the bulk as well as at the air/water interface.[11,12] Ferroelectric packing arrangements could lead to a large in-plane dipolar interaction directed along the layer normal. However, if in-plane antiferroelectric interactions were to dominate, then the hydrocarbon/fluorocarbon contact is realized, leading to the possibility of different types of antiphase behavior.

Studies reported here investigate four model compounds, i.e., 7O.2 SF_5 and 10O.2 SF_5, both of the *para* and *meta* types (see Figure 1). Here the alkyl chain of the *n*O.*m* compounds is replaced by the $SF_5-CF_2-CF_2$ group while the alkoxy chain is hydrocarbon-based (C_7 and C_{10}). Our studies have the benzylidene group in either *para* or *meta* position with respect to the perfluorinated chain. The *meta* structures induce a kink at the center of the molecule. Tilted smectics of bent molecules have

* To whom correspondence should be addressed: Fax 503.725.9525; e-mail ranavas@pdx.edu.
[†] Portland State University.
[‡] California Institute of Technology.
[§] Oregon Health & Science University.
[⊥] University of Oregon.

10.1021/jp047732o CCC: $27.50
Published on Web 12/08/2004

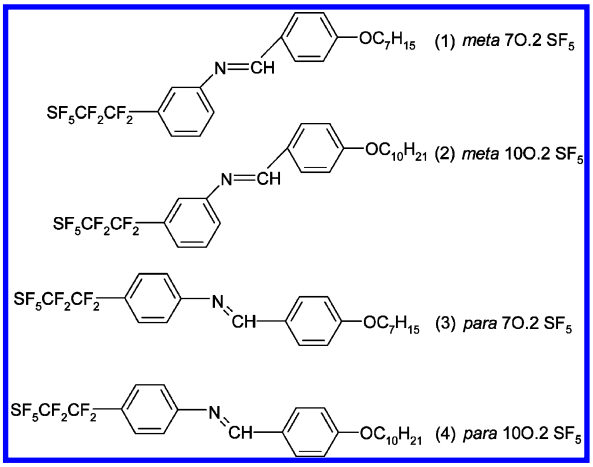

Figure 1. Molecular structure of SF_5-derivatized perfluorinated Schiff base liquid crystals.

recently attracted significant attention due to their novel polarization switching properties. Unlike classic ferroelectric liquid crystals, the bent molecules may be achiral. As long as the overall structural C_2 symmetry (monoclinic) is preserved, it is possible to measure the polarization reversal current associated with the switching in ferroelectric/antiferroelectric structures.[13−16] The bent molecular structure is also important from a theoretical point of view in that such structures exhibit the so-called generalized smecticC (SmC_G) phase (of triclinic symmetry) first predicted by de Gennes[17−19] and recently observed by Heppke et al.[18]

The *para* structures are analogous to the classic *n*O.*m* compounds. The *para* compounds exhibit monotropic nematic and smectic phases. Their mixtures display an enantiotropic nematic phase and monotropic smectic A phase.

Differential scanning calorimetry (DSC) and polarized optical microscopy (POM) studies reveal that the nematic to smectic A (N → SmA) phase transition in both *para* 7O.2 SF_5 and 10O.2 SF_5 is close to second-order. Although 10O.2 SF_5 shows a larger extent of the nematic phase, it exhibits a stronger specific heat anomaly than 7O.2 SF_5. These observations are rationalized using the Landau−de Gennes theory incorporating the effect of the axial dipole moment. Using the single-crystal coordinates of 7O.2 SF_5, several geometry optimizations on representative members of a few liquid crystal homologous series were performed at different levels of theory to evaluate the effect of axial molecular dipole moments on the tricritical point.

The *meta* compounds reveal extraordinarily large hysteresis in the crystal to isotropic phase transition. The magnitude of freezing point depression is consistent with finite size effects on melting of nanosized nucleating crystals, where the rate of crystal growth is extremely slow and is not well understood at present.

Experimental Methods

1. Synthesis of Liquid Crystals. Alkoxyaldehydes were obtained from Frinton Chemicals and were used as received. The Schiff bases were prepared following the established protocol.[20] Recently, we have developed new synthetic routes to prepare *m*- and *p*-$SF_5CF_2CF_2C_6H_4NH_2$ compounds.[21,22]

To prepare the new Schiff bases, equimolar amounts of the reactants *m*- and *p*-$SF_5CF_2CF_2C_6H_4NH_2$ and the appropriate alkoxyaldehyde (C_7 or C_{10}) were added to a 15 mL screw-cap vial equipped with a Teflon stirrer. The reaction mixture was then heated in an oil bath with continuous stirring for 1 h (C_7) and 3 h (C_{10}), and progress of the reaction was monitored with thin-layer chromatography. After condensation, the reaction mixture was separated into pure compounds using column chromatography and recrystallized twice from methanolic solutions.[22,23] The compounds were then characterized by ^{19}F and ^1H NMR, FT-IR, GC-MS, HRMS (high-resolution mass spectroscopy), and elemental analysis. In the case of the *para* 7O.2 SF_5 compound, sufficiently large crystals were obtained that permitted single-crystal X-ray analysis. Additional information regarding the characterization of these molecules is provided in Appendix A of the Supporting Information.

TABLE 1: Crystallographic Information for *Para* 7O.2 SF_5

para 7O.2 SF_5	$C_{22}H_{24}F_9NOS$
formula weight	521.5
crystal system	monoclinic
space group	$P2_1/a$
a, b, c	18.849(4), 5.5418(7), 22.618(3) Å
α, β, γ	90°, 96.956(13)°, 90°
V	2345.2(7) Å^3
Z	4
d_{calc}	1.477 g cm^{-3}
m	2.24 cm^{-1}
F_{000}	1072

2. Differential Scanning Calorimetry. The phase transitions in these molecules were investigated using a Mettler DSC-30 calorimeter interfaced to a PC using Labview software. This interface is a simple 8-bit A/D card operating at 100 kHz and collecting signals from the analog output of a TC10A controller. The Labview software allows one to surpass the data processing capability of the TC10A controller in terms of both the number of data points collected (typically 10−20K) and the overall signal quality (1000 measurements per temperature increment). The heats of transition and transition temperatures were determined using Psi-Plot software, which yielded data precision of 3−4% for first-order phase transitions. Typical runs employed 2 deg/min cooling/heating rates, but in cases where large hysteresis in phase transition temperatures was noted, low cooling rates approaching 0.1 deg/min were used.

3. Polarized Optical Microscopy. These studies were performed on a Zeiss optical microscope equipped with an Instec temperature controller stage allowing for temperature control better than 0.01 °C. Video images of the polarized optical textures were captured using a Kodak CCD camera (MDS100) interfaced to a laptop PC.

4. Small-Angle X-ray Diffraction (SAXS). The method and instrument used for this analysis are described elsewhere.[24] Samples were sealed in 1 mm Mark capillaries. Temperature control was obtained using a platinum sensor and a phase locked loop temperature controller to provide temperature control better than 0.1 °C.

5. Single-Crystal X-ray Studies. *Crystal Structural Analysis.* A crystal of dimensions 0.08 × 0.29 × 0.54 mm cleaved from a longer specimen was mounted on a fiber with epoxy. Attempts to cool crystals to 146 K resulted in cracking and deterioration. The orientation parameters and cell dimensions were obtained at 221 K from the setting angles of a Nonius CAD-4 serial diffractometer for 25 centered reflections in the range $11.2° \leq \theta \leq 13.0°$. Table 1 contains a summary of crystal data and the final residuals.

A more extensive table including particulars of data collection and structure refinement is in the Supporting Information. The systematic absence of reflections and monoclinic Laue symmetry indicated the space group $P2_1/a$. Absorption corrections were not applied. There was no systematic change in the intensities of control reflections during data collection. A SIR92 E-map[25] showed all the non-hydrogen atoms. Nearly all hydrogen atoms were apparent in a difference synthesis; all were included at

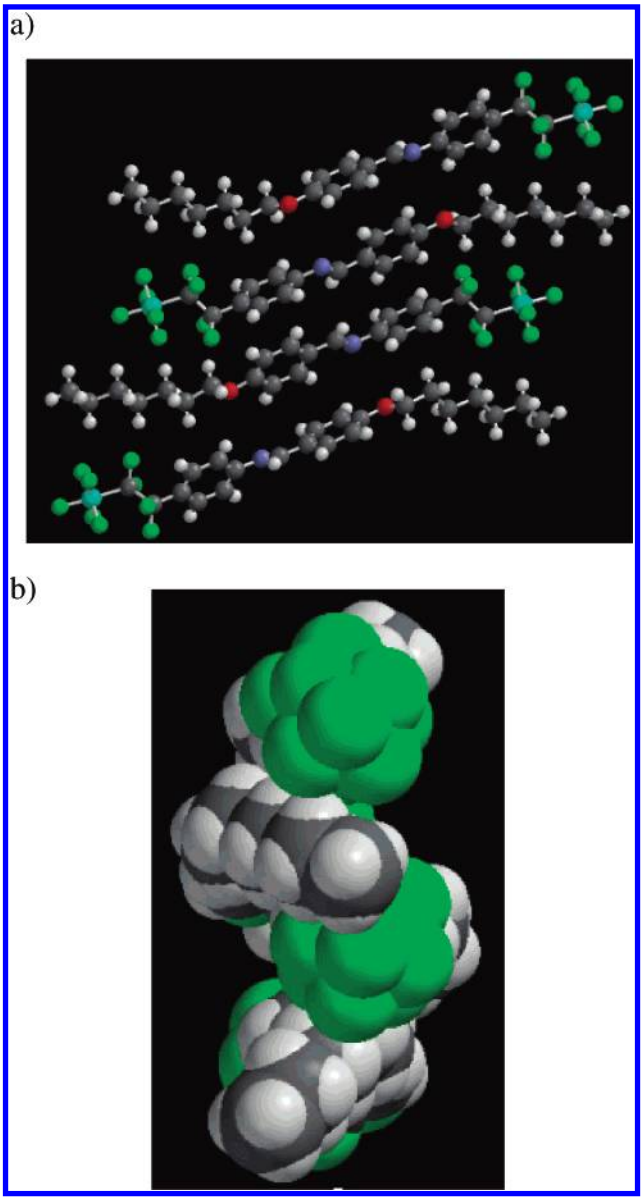

Figure 2. Ball-and-stick model and space-filling model 7O.2 SF_5 depicted in (a) $a-c$ plane and (b) $a-b$ plane rendered with Spartan.

positions recalculated after each cycle of refinement [B(H) = 1.2B_{eq}(C); d(C−H) = 0.95 Å]. The final difference synthesis was featureless. The TEXSAN program suite[26] was used in all calculations.

The unit cell contains four molecules in a slightly staggered state with antiferroelectric arrangement with respect to polar SF_5 groups. Furthermore, the alkoxy chain has a gauche bond about C_x-C_y bond and the two benzene rings are not coplanar. This is shown in Figure 2.

Using the atomic coordinates from the single-crystal data, geometric packing of the molecules was generated using the Molecule software package.[26] The unit cell is depicted in Figure 2a (ball-and-stick model of the $a-c$ plane) and Figure 2b (space filling molecule of the $a-b$ plane). Note the "mixing" of perfluorinated and hydrocarbon chains.

6. Computational Methods. Two distinct computational methods were utilized in this work to determine the equilibrium geometries and permanent dipole moments of 7O.2, 10O.1, 7O.2 SF_5, 10O.2 SF_5, 10S5, 9OCB, 10OCB, 9CB, and 10CB. These methods included the traditional Hartree−Fock theory and B3LYP variant of density functional theory. The B3LYP functional combines the hybrid three-parameter exchange functional of Becke[27] and the correlation functional of Lee, Yang, and Parr.[28] In all computations, the 6-31G* basis set was employed. The grid used in the geometry optimizations was the default-pruned grid with 75 radial shells and 302 angular points per shell. Optimized structures were found with Cartesian forces less than 4.5×10^{-4} hartrees/bohr. All computations were performed using the Gaussian 98[29] suite of programs, and the final Cartesian coordinates are provided in the Supporting Information.

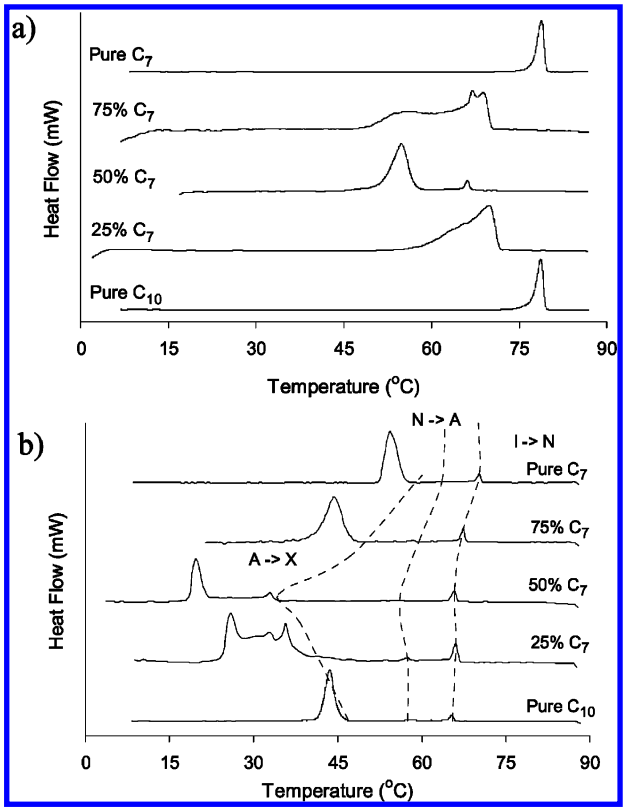

Figure 3. DSC thermograms (average of three trials) of *para* 7O.2 SF_5 and 10O.2 SF_5 mixtures for (a) heating and (b) cooling runs. Heat flow (in mW) numbers representing the true values of the maximum peak [from bottom to top] are as follows: (a) 5.92, 1.09, 1.15, 0.75, 5.92 and (b) 3.55, 0.69, 1.49, 1.26, 2.82.

TABLE 2: Thermodynamic DSC Data for the Cooling of *Para* 7O.2 SF_5 and 10O.2 SF_5 Mixtures[a]

mole fraction of C_{10}	McMillan parameter (T_{NA}/T_{NI})	transition temp (°C) [ΔH (kJ/mol)]		
		I → N	N → SmA	SmA → X
0	0.978	69.6 (1) [1.6 (1)]	62.1 (2)	52.5 (1) [24.5 (8)]
0.24	0.971	66.8 (4) [1.06 (3)]	56.8 (8)	40.1 (4) [17 (1)]
0.48	0.967	64.8 (1) [1.44 (6)]	53.6 (2)	31.1 (6) [17.4 (9)]
0.74	0.971	65.6 (5) [1.00 (4)]	55.8 (7)	33.8 (2) [19.3 (6)]
1	0.976	64.7 (1) [1.4 (2)]	56.7 (2)	41.9 (4) [25.1 (9)]

[a] Numbers in parentheses give standard deviations for the last quoted digit.

Results and Discussion

The DSC thermograms for *para* compounds and their mixtures, presented in Figure 3, exhibit several monotropic transitions. The measured heats of transition and transition temperature uncertainties are provided in the accompanying Table 2. The *meta* compounds, however, do not exhibit as many transitions but undergo a remarkable degree of undercooling (see Figure 4).

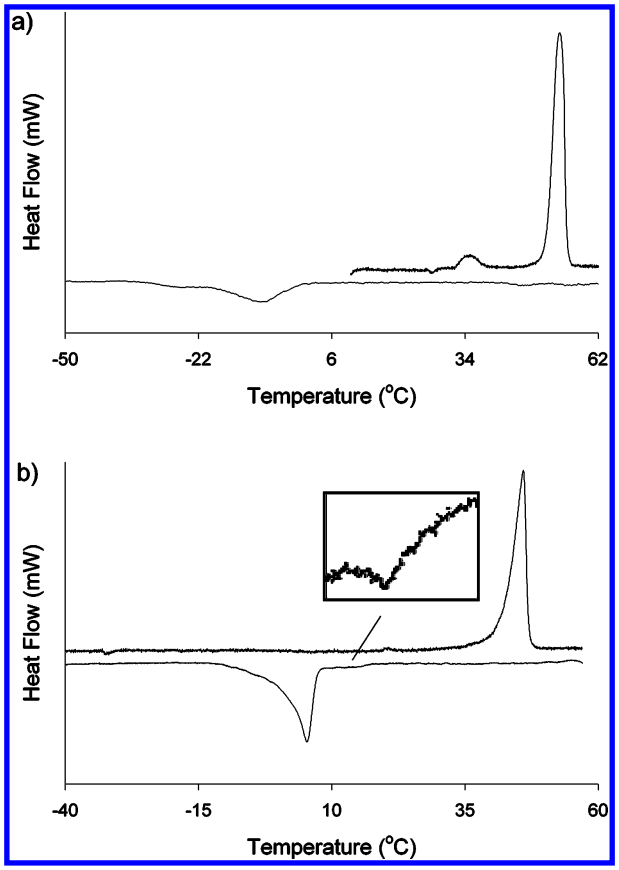

Figure 4. DSC heating and cooling thermograms of pure *n*O.2 SF_5 compounds for *meta* (a) 7O.2 SF_5 and (b) 10O. 2 SF_5. Both heating and cooling was performed at a rate of 2 deg/min. Inset shows onset of monotropic I → liquid crystal transition at 15 °C. The upper trace in (a) and (b) depicts the heating scans, while the bottom trace illustrates the cooling scans.

A. *Para* 7O.2 SF_5. The transition enthalpy of the peak at 69.6 °C is 1.6 kJ mol^{-1} and is typical of an isotropic → nematic (I → N) transition (0.8−1.5 kJ/mol).[30−32] Shown in Figure 5 are the optical textures of *para* 7O.2 SF_5 exhibiting nematic and smecticA textures.[33] In polarized microscopy, classic nematic schlieren textures[33] are observed below 69.6 °C (see Figure 5a). Upon further cooling nematic textures evolve into a focal conic texture at lower temperature (62.1 °C); this is a characteristic of the smectic A phase.

The nematic → smectic A (N → SmA) phase transition is barely visible in the calorimetry study, implying a very weak first-/second-order transition (see Figure 6). The lower temperature DSC peak (52.5 °C) has a relatively high heat of transition and is perhaps a smectic A → crystal (SmA → X) transition. However, it also exhibits a small shoulder prior to this transition, which could be due to a smectic A → smectic B (SmA → SmB) transition.

A direct analogue of the phase sequence based on the molecular length consideration would be with the hydrocarbon 7O.3 compound. The phase sequences of a few members of the 7O.*m* series follow:

$$\text{7O.1 I} \xrightarrow{70} \text{N} \xrightarrow{61} \text{SmA} \xrightarrow{56.8} \text{SmB} \xrightarrow{50} \text{X}$$

$$\text{7O.2 I} \xrightarrow{69} \text{N} \xrightarrow{65} \text{SmA} \xrightarrow{59} \text{SmB} \xrightarrow{57[22\ \text{kJ}]} \text{X}$$

$$\text{7O.3 I} \xrightarrow{80.5} \text{N} \xrightarrow{73} \text{SmA} \xrightarrow{49} \text{SmF} \xrightarrow{48} \text{SmB} \xrightarrow{39[23\ \text{kJ}]} \text{X}$$

$$\text{7O.2 } SF_5\text{(new) I} \xrightarrow{70} \text{N} \xrightarrow{62} \text{SmA} \xrightarrow{53} \text{SmB(?)} \xrightarrow{52[23\ \text{kJ}]} \text{X}$$

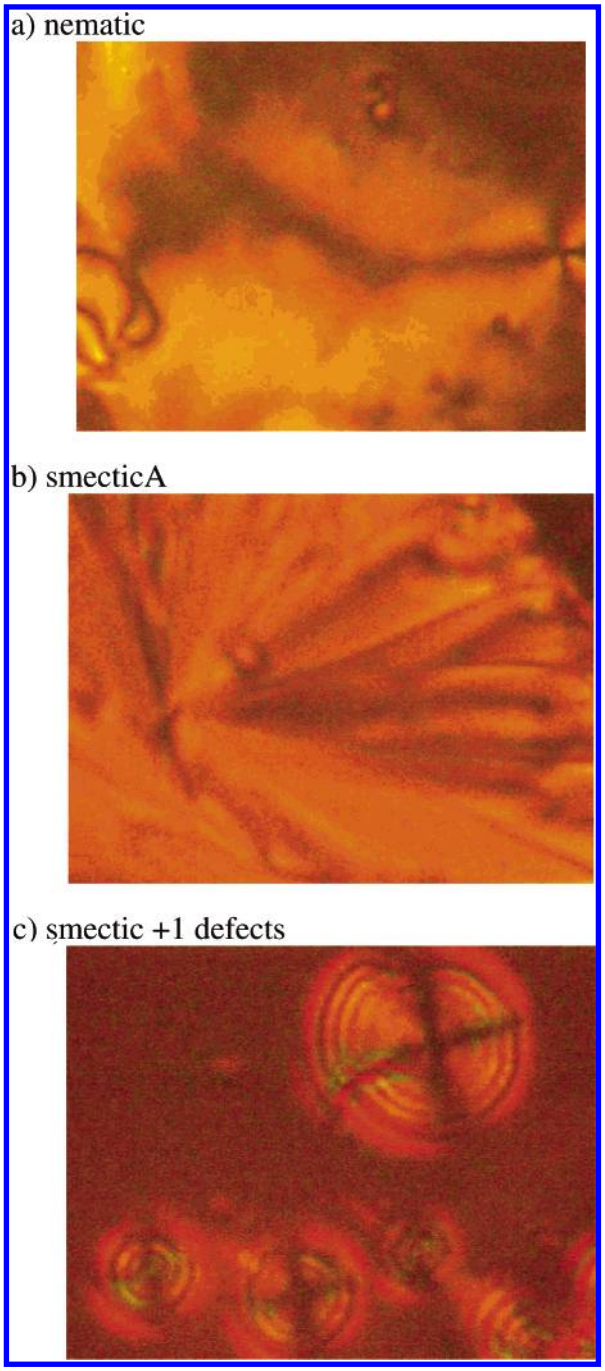

Figure 5. Nematic and smectic A textures observed in SF_5-based compounds. Notice the +1 and $-^1/_2$ defects of nematics (*para* 7O.2 SF_5 at 69.6 °C). Upon cooling, the sample transformed into a smectic phase exhibiting focal conic texture (62 °C) (magnification 80×).

Clearly, an introduction of an SF_5 group in conjunction with two CF_2 groups leads to identical phase sequence as in the case of 7O.2, since we do not observe a SmF phase that is detected in hydrocarbon 7O.3. The identity of the SmB phase is uncertain at this time, owing to the narrow extent of the phase. The monotropic nature of these mesophases makes it difficult to observe the textures of this smectic phase owing to its rapid crystallization. Note that the phase sequences of the *n*O.*m* compounds depicted above reveal that these compounds generally exhibit SmB → X for lower ($n < 4$) alkyl chain lengths with heat of freezing of about 20−26 kJ mol^{-1}. Higher chain homologues, which exhibit the SmG → X transition, typically have heats of transition that are higher than 40 kJ/mol.

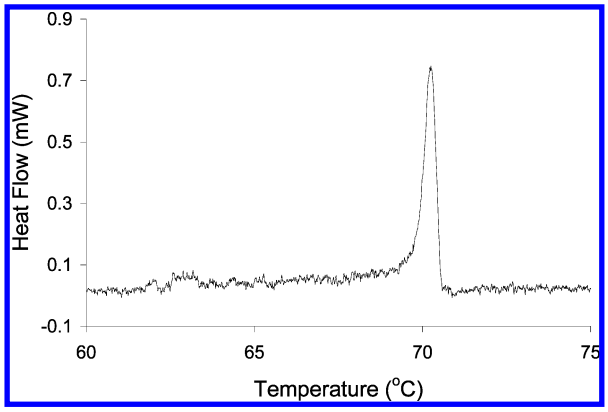

Figure 6. DSC cooling thermogram of pure *para* 7O.2 SF_5.

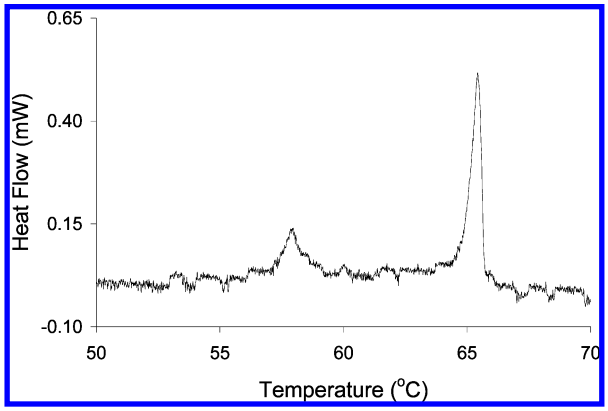

Figure 7. DSC cooling thermogram of pure *para* 10O.2 SF_5.

B. *Para* 10O.2 SF_5. This compound also exhibits a sequence of similar monotropic phases. However, the N → SmA transition is now much stronger, having a discernible specific heat anomaly (see Figure 7).

Comparing the phase sequence with the hydrocarbon 10O.*m* series, we find that its phase sequence is comparable to 10O.1, since the nematic phase is observed only in 10O.1.

$$10O.1\ I \rightarrow N \rightarrow SmA \rightarrow X$$

$$10O.2\ SF5(new)I \xrightarrow{65} N \xrightarrow{57} SmA \xrightarrow{42} X$$

$$10O.2\ I \rightarrow SmA \rightarrow SmB \rightarrow SmG \rightarrow X$$

The lowest temperature mesomorphic phase is a SmG phase for $m > 1$; SmA → X and SmB → X transitions are observed for 10O.1 and 10O.3, respectively. Remarkably, the presence of SF_5 groups and CF_2 groups affects insignificantly the phase sequences of parent *n*O.*m* compounds. This is in stark contrast to previous work, where direct replacement of the CN group by SF_5 group of known liquid crystal structures was reported.[1,6] Overall, the tendency is to shift the phase sequence in the direction of lower *m*. This is unexpected in that the chain contribution to dispersive interactions of typical CF_2 groups is expected to be larger than of the CH_2 group, indicating a compensating role played by the SF_5 group.

Observation of a nematic phase in these compounds is consistent with recent numerical simulations (using molecular dynamics (MD) and Monte Carlo (MC) methods) of liquid crystalline phases using Gay-Berne potentials.[34] For modest length-to-breadth ratios, movement of the molecular dipole from the center to the end of the molecule increases T_{NI}. In view of the importance of electrostatics on the extent of nematic and smectic phases, we conducted computational simulations of the dipole moments (see below).

The second-order nature of the N → SmA phase transition in these two compounds is unexpected. A change in the order of the N → SmA transition[8,35] has been noted in the *n*O.*m* (first (second) order for $n \geq 6$ ($n < 5$)) series.[30] Within experimental resolution both first- and second-order N → SmA transitions occur and are separated by a tricitical point (TCP), as was predicted many years ago by de Gennes and McMillan.[17] Both the Landau and molecular field theories emphasize the important role played by the coupling between the nematic and smectic-order parameters. They predict that materials exhibiting a shorter nematic phase extent should exhibit a first-order N → SmA transition. The crossover between the first- and second-order region is quantified by the tricritical McMillan parameter, M_{TCP} [$= (T_{NA}/T_{NI}) = 0.87$]. Various homologous series of liquid crystals exhibit tricritical N → SmA points.[32,35,36] However, there is no universal value for M_{TCP}; it varies from system to system from about 0.93−0.98 for monolayer (≤0.99 for "partial" bilayer) forming systems.

7O.2 SF_5 ($M = 0.978$) has a weaker specific heat anomaly for the N → SmA transition than the 10O.2 SF_5 ($M = 0.976$) despite its smaller nematic phase extent. Similar behavior has been noted by Pisipati et al.[30] in *n*O.*m* compounds (5O.6, $M = 0.968$ weak first order and 6O.5 $M = 0.972$ strong first order) where compounds having identical nematic phase extents (essentially identical McMillan parameter) exhibit either first- or second-order transition.[30] The order of the transition appears to be controlled by the length of the polar alkoxy chain.[30] One may rationalize the behavior using the Landau−de Gennes theory of the N → SmA transition. In this theory, the sign of the fourth-order term,[8] b, governs the order of the transition ($b = b_0 - {}^1/_2c^2\chi_{NI}$), where χ_{NI} [$\approx \chi_0(T_{NI}/(T_{NI} - T_{NA}))$] is the nematic susceptibility at the N → SmA transition, while c is the coupling coefficient between the nematic and the smectic order parameters.[35] Coupling of the nematic order parameter fluctuation with the smectic order gives a first ($b < 0$), second ($b > 0$), or tricritical ($b = 0$) N → SmA transition. Nevertheless, it is conceivable that in the lowest order c (see eq 1) would depend inversely on the axial molecular dipole moment μ_x, implying that a larger dipole moment effectively suppresses the effect of nematic susceptibility fluctuations. Therefore, the coefficient of the fourth-order term can become positive despite the smaller extent of the nematic phase

$$c = \frac{\alpha}{\mu} \tag{1}$$

$$M_{TCP} = 1 - \frac{c^2\chi_0}{2b_0} = 1 - \frac{\alpha^2\chi_0}{2b_0}\frac{1}{\mu^2} \tag{2}$$

The scaling form of c as presented in eq 1 was established by considering the following limits. When $\mu \rightarrow \infty$, the M_{TCP} should tend to 1, forcing the disappearance of the tricritical point (nematic phase). In the other extreme, when $\mu \rightarrow 0$, the $M_{TCP} < 0$, indicating suppression of TCP below 0 K (i.e., disappearance of the smectic phase). The constants α, χ_0, and b_0 are expected to depend on other molecular parameters such as chain−chain interactions. From these considerations, it becomes clear that a universal value of M_{TCP} would not be expected.

To probe the functional dependence of the M_{TCP} on the axial molecular dipole moment, we have performed quantum chemical calculations on typical liquid crystal homologous series [7/10O.2, 9/10CB, 9/10OCB, 7/10O.2 SF_5, and 10S5] as shown in Table 3.

TABLE 3: Dipole Moments for Selected Liquid Crystals[a]

	HF/6-31G* (B3LYP/6-31G*)			
compound	μ_x	μ_y	μ_z	μ_{total}
7O.2	1.4 (1.9)	2.3 (2.0)	1.4 (1.1)	3.0 (3.0)
9CB	5.8 (5.8)	1.6 (1.6)	0.4 (0.4)	6.0 (6.0)
9OCB	6.7 (7.1)	0.02 (0.2)	0.02 (0.02)	6.7 (7.1)
10CB	5.7 (5.7)	1.9 (1.8)	0.3 (0.4)	6.1 (6.0)
10O.1	1.2 (1.6)	2.3 (2.2)	1.6 (1.2)	3.0 (3.0)
10OCB	6.7 (7.1)	0.07 (0.2)	0.03 (0.04)	6.7 (7.1)
10S5	2.0 (2.8)	0.8 (0.8)	0 (0.1)	2.1 (2.9)
7O.2 SF_5	6.9 (8.3)	2.6 (2.3)	1.0 (0.8)	7.5 (8.6)
10O.2 SF_5	6.4 (7.8)	2.7 (2.7)	1.6 (1.1)	7.2 (8.4)

[a] Dipole moments are in units of debye. Estimated uncertainty in the calculated vs experimentally observed dipole moments using these computational methods is about ±0.3 D. Along the *x*-direction, these molecules exhibit lowest moment of inertia; so the *x*-coordinate is approximately parallel to the molecular long axis.

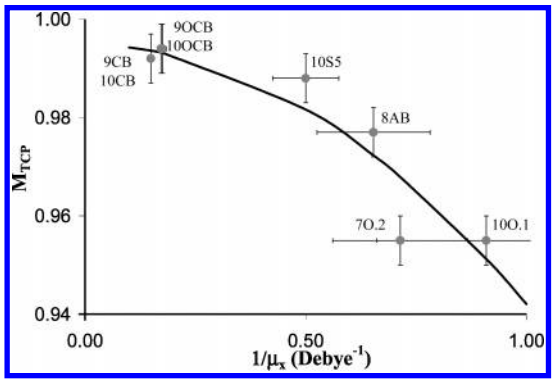

Figure 8. Dependence of M_{TCP} vs $1/\mu_x$ employing the HF/6-31G* computational method. The behavior is described by $M_{TCP} = [0.995 \pm 0.003] - [0.054 \pm 0.009]/\mu_x^2$ with a $\chi^2 = 0.9$. The B3LYP/6-31G* method (not illustrated in the figure) is presented by $M_{TCP} = [0.990 \pm 0.003] - [0.04 \pm 0.02]/\mu_x^2$ and with a $\chi^2 = 0.6$.

The optimized coordinates, moments of inertia, and stabilization energies for these compounds appear in the Supporting Information. Figure 8 shows how M_{TCP} (obtained from literature sources)[23,30,35,36] varies with $1/\mu_x$ (computed), which is consistent with the scaling form of *c* presented in eq 1. Thus, two liquid crystals having identical nematic phase extent but different molecular dipole moments can exhibit first- or second-order N → SmA transition. (Precise dependencies of the Landau coefficients on the molecular parameters such as dipole or quadrupolar moments are unknown. Furthermore, the values of these moments, as calculated, are susceptible to small changes in bond angles and distances; therefore, our suggestion that *c* scales inversely with the dipole moment should only be considered qualitatively.)

The predicted M_{TCP} values for *para* 7O.2 SF_5 and *para* 10O.2 SF_5 lie between 0.994 and 0.995 much greater than the experimental *M* values (0.978 and 0.976), suggesting second-order N → SmA transitions. Calculated M_{TCP} values are closer to those of a "partial" bilayer SmA forming molecules and are even greater than M_{TCP} values found for cyanobiphenyls.[36]

X-ray Diffraction Studies. To probe how the lateral chain−chain interactions affect the molecular packing, the single-crystal structure of *para* 7O.2 SF_5 was investigated. The observed crystal structure (see Figure 2) is similar to an antiphase structure predicted by Prost[8] and experimentally observed by Levelut et al.[9] More specifically, alternating arrangements of SF_5 groups in a single monolayer has a periodicity of $q_x \approx 2\pi/b = 2\pi/5.5$ Å. Since the molecules in the crystal structure have a tilt of 6°, this structure is similar to the frustrated SmĈ (in the Prost notation). Clearly more studies of higher fluorocarbon chain length would be necessary to establish the occurrence of the frustrated SmĈ; such studies are currently in progress. Figure 9 presents

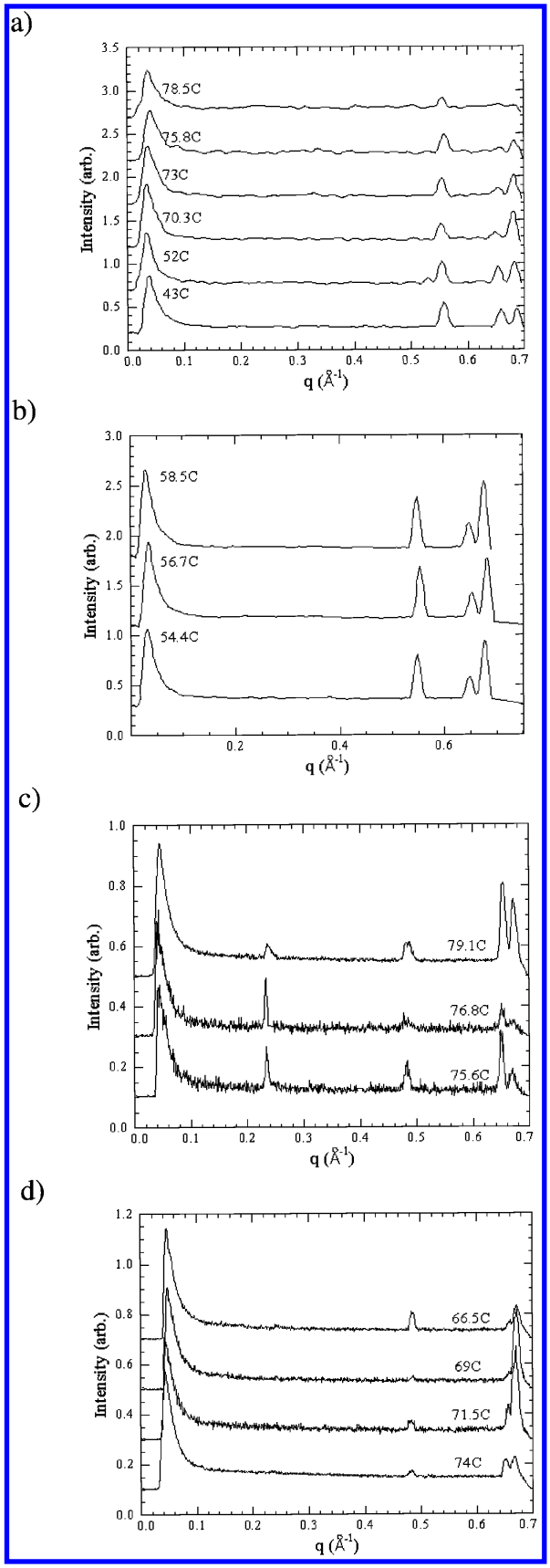

Figure 9. Variable temperature diffraction patterns for *para* 7O.2 SF_5 for (a) heating and (b) cooling runs and for *para* 10O.2 SF_5 during (c) heating and (d) cooling.

TABLE 4: Miller Indices and Corresponding *d* Spacing Parameters for 7O.2 SF_5 and 10O.2 SF_5 Compounds

Miller indices	*para* 7O.2 SF_5 *d* spacing (Å)	*para* 10O.2 SF_5 *d* spacing (Å)
0, 0, 1	*a*	26.1
0, 0, 2	11.4	12.9
2, 0, 0	9.7	9.6
2, 0, −1	9.3	9.4

[a] "Not observed".

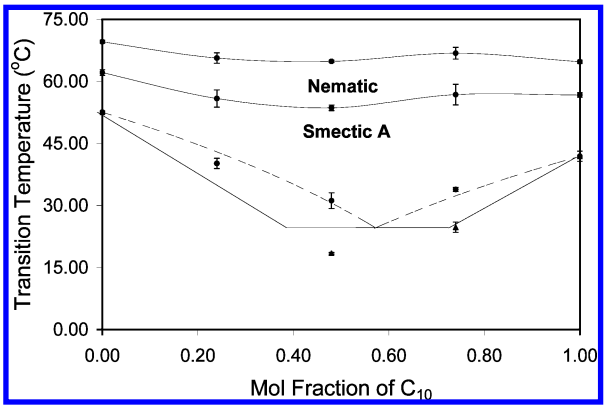

Figure 10. Phase sequence observed in *para* 7O.2 SF_5 and 10O.2 SF_5 compounds determined from DSC cooling scans. The dashed lines (smectic A → crystal phase transition) were calculated using the Van't Hoff relation.

the variable temperature diffraction data during the cooling and heating of the *para* compounds. The assignment of the Miller indices presented in Table 4 is based on the crystal structure of *para* 7O.2 SF_5.

The observed line shapes are characteristic of crystals, and some modulation of the relative intensities is observed near the X → I transition(s). Notably, the 001 peak for *para* 7O.2 SF_5 molecule is absent. The intensity for this peak was verified using the Texscan powder diffraction simulation program. It was found that the intensity corresponding to the 001 peak in comparison with the 002 peak is an order of magnitude weaker. 10O.2 SF_5 on virgin heating did show 001 reflection. However, during cooling runs its intensity was extremely weak. The overall diffraction pattern within the q range accessible on SAXS instrument bears striking resemblance to 7O.2 SF_5; hence, we have assigned Miller indices as shown in Table 4. Note the above data do not show scattering characteristics of nematic or smectic phases, implying rapid crystallization of these compounds on the time scale of experimental measurements.

C. Binary Mixtures of 7O.2 SF_5 and 10O.2 SF_5 Compounds. Both 7O.2 SF_5 and 10O.2 SF_5 exhibit monotropic liquid crystal phases; hence, whether enantiotropic phases can be obtained in their binary mixtures was examined using DSC (see Figure 3). The resulting phase sequences are presented in Figure 10, which depicts enantiotropic nematic phases but not the smectic phase.

Heating Scans. The sharp crystal melting peak observed in the pure components is shifted toward lower temperature and shows considerable broadening. For midrange compositions, it eventually splits into two peaks corresponding to the I → N and N → X phase transition (see Figure 3a).

Cooling Scans. Cooling theromgrams *para* C_7/C_{10} mixtures are presented in Figure 3b. The results are summarized in Figure 10. They show (1) a complete miscibility in the monotropic nematic and smecticA phases and a partial miscibility in the crystalline/solid phase, (2) an injection of the enantiotropic nematic phase at about 50% composition, and (3) almost 50 °C depression in crystal freezing temperature near the midrange of composition of the binary mixture.

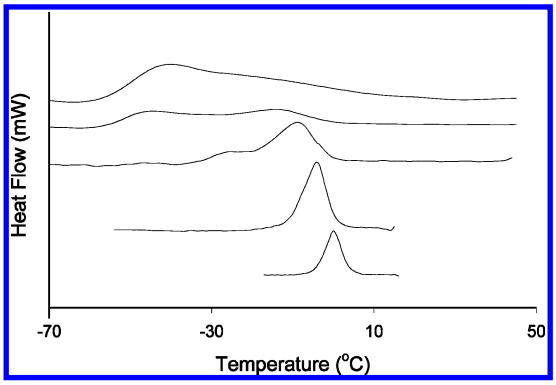

Figure 11. *Meta* 7O.2 SF_5 DSC cooling runs at variable cooling rates [from top to bottom: 10°, 5°, 2°, 1°, and 0.5°]. The individual plots have been shifted upward for a better representation.

The SmA → X crystal transition in cooling runs is broad and allows one to determine the SmA → X coexistence range. The calculated (dotted) lines go through the experimentally determined onset temperatures for this transition. Although the above data are consistent with the Van't Hoff relationship, the validity of this approach for monotropic transitions has not been established.

D. *Meta* 7O.2 SF_5. Since the benzylidine group is located in the *meta* position, there are no hydrocarbon analogues for this series of compounds. The phase transition observed at 55 °C exhibits hysteresis over a 50 °C interval (see Figure 4a)! The magnitude of ΔH (30.9 kJ mol^{-1}, $T_{X\rightarrow I} = 55$ °C) is an indicator of an X → I transition. Once melted, the isotropic phase is stable at room temperature over periods of weeks. Even when crystal nuclei are formed, the rate of their growth is extraordinarily slow.

The degree of undercooling clearly depends on the cooling rate. DSC thermograms at various cooling rates ($\Delta H = 25$ kcal mol^{-1}, $T_{I\rightarrow X} \approx -5$ °C) are presented in Figure 11. The classical homogeneous nucleation theory predicts that the nucleation barrier should depend on the interfacial tension between the melt and crystal/liquid crystal phase and the degree of undercooling, $\Delta G_{nucleation} \propto \sigma^3 \nu^2 (T_m/\Delta H \Delta T)^2$, where σ is the surface tension, ν is the molecular volume, and ΔT is the degree of undercooling.[34] Its origins may lie in the details of the molecular packing and the size of the critical nucleating cluster. The size-dependent depression of freezing point is given by[37]

$$T_\infty - T_m = \frac{2T_\infty}{L}\left\{\frac{\sigma_1}{\rho_1(r-t_0)} + \frac{\sigma_2}{r}\left(\frac{1}{\rho_1} - \frac{1}{\rho_2}\right)\right\} \qquad (3)$$

where T_∞ and T_m are the bulk melting and the observed freezing temperatures. Furthermore, $\rho_{1,2}$ are the densities of the solid and liquid phases and $\sigma_{1,2}$ are the solid−liquid and liquid−air surface tensions, respectively, L ($\equiv \Delta H_m$) is the heat of melting, and t_0 is the thickness of ordered liquid surrounding the nucleating cluster. Estimating σ_1 (from the Turnbull equation[34] $\sigma_{LS} = C\Delta H_m \rho_s^{2/3}/N_A^{1/3}$ [for nonmetallic solids $C = 0.32$], where ρ_s is the number density in mol m^{-3} and N_A is Avogadro's number) yields a value of 0.017 J m^{-2}.

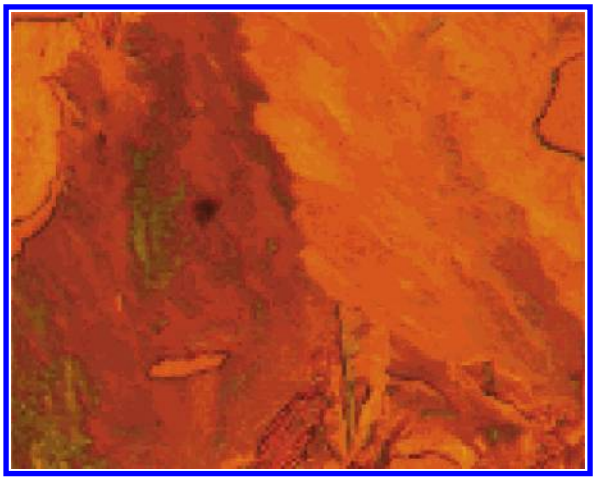

Figure 12. Optical textures of *meta* 10O.2 SF_5 exhibiting a smecticF phase (magnification 80×).

Neglecting the second term, one can estimate the order of magnitude for $r - t_0$, the size (independent of ΔH_m) of the nucleating crystal as given in eq 4:

$$r - t_0 = \frac{2T_\infty C}{(T_\infty - T_m)\sqrt[3]{\rho_1 N_A}} \tag{4}$$

Since $\rho_s = 1.82 \times 10^3$ mol m^{-3}, $\Delta T = 60$ K, and $T_\infty = 328$ K, the $r - t_0$ value is approximately 3 nm, consistent with typical dimensions of the unit cell ($2.2 \times 1.8 \times 0.5$ nm^3). At room temperature, where $\Delta T = 30$ K, $r - t_0$ would be 7 nm. The dimension of the nucleating cluster allows evaluation of the rate of nucleation (I) using the classic nucleation theory:[38]

$$I = \frac{N_A kT}{h}\exp\left(-\frac{\Delta G_D}{kT}\right)\exp\left(-\frac{4\pi\sigma_{LS}r^2}{3kT}\right) = 10^{33}\exp\left(-\frac{4\pi\sigma_{LS}r^2}{3kT}\right) \tag{5}$$

where ΔG_D (≈ 2 kJ mol^{-1}) is the free energy for diffusion. Using $\Delta H = 30\,900$ J mol^{-1}, $I = 1.08 \times 10^{-344}$ nuclei cm^{-3} s^{-1}. This explains the remarkable stability of the isotropic phases at room temperature; however, at $\Delta T = 60$ K $I = 1.03 \times 10^{-44}$ nuclei cm^{-3} s^{-1}. These values are extremely sensitive to the estimated liquid−solid interfacial tension. For instance, if $\sigma_1 = 0.008$ J m^{-2} and $r - t_0 = 1.5$ nm, the nucleation rate for $\Delta T = 60$ K is 3.20×10^{24} nuclei cm^{-3} s^{-1}.

Such considerations should also apply to hydrocarbon liquid crystal homologues when one is dealing with I → X transition. However, it is rare to observe such a high degree of undercooling due to heterogeneous nucleation.[39] In this case the nucleation barrier is reduced for the contact angle $\theta < \pi/2$ ($\Delta G \propto 1/2\sigma_{LS}$-$(1 - \cos\theta - {}^1/_2 \cos\theta \sin^2\theta)$),[40] thereby increasing the nucleation rates as discussed above. If the isotropic phase of the fluorinated liquid crystals does not wet the surface (i.e., $\cos(\theta) \approx -1$), a homogeneous nucleation mechanism may prevail. A similar trend is also observed in *para* compounds, which exhibit a high degree of undercooling with I → X transition leading to the appearance of monotropic liquid crystal phases in the supercooled region.

E. *Meta* 10O.2 SF_5. The calorimetric data for this compound suggests a monotropic isotropic to mesophase transition. The optical texture studies (see Figure 12) indicate that this mesophase is likely to be a smectic F phase. Just as in the case of its lower chain homologue, a significant undercooling is observed.

Using the previous approach, for $\Delta H_m = 42\,000$ J mol^{-1}, $\rho_s = 1.69 \times 10^3$ mol m^{-3}, $\sigma_{LS} = 0.0226$ J m^{-2}, $\Delta T = 36$ K ($\Delta T = 21$ K, room temperature), and $T_\infty = 319$ K, the $r - t_0$ value is 6 nm (10 nm). The corresponding nucleation rate is 1.32×10^{-303} nuclei cm^{-3} s^{-1} (1.13×10^{-955} nuclei cm^{-3} s^{-1}). These low nucleation rate estimates suggest that the transition from an isotropic to a crystalline phase is interrupted by a monotropic mesophase. Higher resolution DSC traces (see Figure 4b, inset) reveal a I → SmF transition consistent with the optical textures presented above. Thus, an increased alkyl chain length in the *meta* series introduces a monotropic liquid crystalline phase.

Viney et al.[41,42] also reported such higher order smectic phases in partially fluorinated diblock hydrocarbon systems. For example, a diblock $C_{10}H_{23}C_{10}F_{23}$ molecule exhibits a tilted smectic G(J) → isotropic phase transition and at lower temperature transition to a biphasic liquid crystalline region. The latter transition exhibited a remarkably slow kinetics of transformation, which appears to be a characteristic of partially fluorinated functional groups in their molecular architecture.

Conclusion

For the first time significant liquid crystals, incorporating the $SF_5-CF_2-CF_2$ functional group in a *n*O.*m* homologous series, are presented. They exhibit remarkably low perturbation of the phase sequence of the parent series, thus providing valuable components for optimizing liquid crystal mixtures. Quantum chemical calculations reveal high molecular dipole moments, even surpassing the high dipole moments observed in the classic cyanobiphenyl homologous series. It is suggested that this molecular feature may drive the observed N → SmA transition in this series closer to a second-order transition despite the higher alkyl chain length. Moreover, the single-crystal structure exhibits a quasi-monolayer structure involving antiferroelectric in-plane ordering, reminiscent of a SmĈ phase. The high degree of *meta* stability for these fluoro-hydrocarbon liquid crystals is ascribed to unfavorable wetting interaction, forcing a slower homogeneous nucleation growth mechanism. Future studies involving an increase in the fluorocarbon chain length and an alteration in the location of the SF_5 group on the molecular architecture would be valuable in order to realize higher order smectics as well as enantiotropic liquid crystals. Preliminary studies of mixtures of these compounds displayed an enantiotropic nematic phase.

Acknowledgment. J.A.S., R.W.W., and G.L.G. are grateful for research support from The Camille and Henry Dreyfus Foundation, Inc., under Grant SI-03-026. S.B.R. and N.A.H. thank Avery Dennison and NIH (Grant No. GMMEDOO18C and GMMEDOO47A) for financial support.

Supporting Information Available: Experimental details, reaction conditions, and purification data, ^{1}H NMR and ^{19}F NMR data, IR data, GC-MS data, optimized atomic coordinates of selected liquid crystals, and crystallographic information. This material is available free of charge via the Internet at http://pubs.acs.org.

References and Notes

(1) (a) Poetsch, E. *Kontakte* (*Darmstadt*) **1998**, 15−28. (b) Kirsch, P.; Poetsch, E. *Adv. Mater.* **1998**, *10*, 602−606.

(2) Riswoko, A. *IECI Jpn. Ser.* **2001**, *3*, 15−21.

(3) Takatsu, H.; Takehara, S.; Takeuchi, K.; Iwashita, Y. *DIC Technol. Rev.* **2002**, *8*, 33.

(4) Takenaka, S.; Okamoto, H. *Ekisho* **2000**, *4*, 3.

(5) Skelton, G. W.; Brett, P.; Jones, J. C.; Kelly, S. M.; Minter, V.; Tuffin, R. P. *Liq. Cryst.* **2001**, *28*, 417−435.

(6) Kirsch, P.; Bremer, M.; Heckmeier, M.; Tarumi, K. *Angew. Chem., Int Ed.* **1999**, *38*, 1989−1992.

(7) Demus, D.; Goodby, John, W.; Gray, G. W.; Spiess, H. W.; Vill, V. *Handbook of Liquid Crystals;* Wiley-VCH Verlag: Weinheim, Germany, 1998; Chapter 6. (b) Kelker, H.; Hatz, H. *Handbook of Liquid Crystals;* Verlag Chemie: Weinheim, Germany, 1980.

(8) Prost, J.; de Gennes, P. G. *The Physics of Liquid Crystals*; Oxford University Press: New York, 1995; Chapter 10.

(9) (a) Sigaud, G.; Hardouin, F.; Achard, M. F.; Levelut, A. M. *J. Phys. (Paris)* **1981**, *42*, 107. (b) Hardouin, F.; Nguyen, H. T.; Achard, M. F.; Levelut, A. M. *J. Phys., Lett.* **1982**, *43*, L327−L381.

(10) Martínez-Miranda, L. J.; Kortan, A. R.; et al. *Phys. Rev. Lett.* **1986**, *56*, 2264−2267.

(11) (a) Takiue, T.; Siegel, S.; Vollhardt, D. *Colloids Surf. A* **2002**, *198*−*200*, 797−804. (b) McCabe, C.; Galindo, A.; Gil-Villegas, A.; Jackson, G. *J. Phys. Chem. B* **1998**, *102*, 8060−8069. (c) Oda, R.; Huc, I.; Danino, D.; Talmon, Y. *Langmuir* **2000**, *16*, 9759−9769.

(12) Scott, R. L. *J. Am. Chem. Soc.* **1948**, *70*, 4090−4093.

(13) Nakata, M.; Link, D. R.; Thisayukta, J.; Takanishi, Y.; Ischikawa, K.; Watanabe, J.; Takezoe, H. *J. Mater. Chem.* **2001**, *11*, 2694−2699.

(14) Niori, T.; Sekine, T.; Watanabe, J.; Takezoe, H. *J. Mater. Chem.* **1996**, *6*, 1231−1234.

(15) Link, D. R.; Natale, G.; Shao, R.; Maclennan, J. E.; Clark, N. A.; Karblova, E.; Walba, D. M. *Science* **1997**, *278*, 1934.

(16) Walba, D. M.; Körblova, E.; Shao, R.; Maclennan, J. E.; Link, D. R.; Glaser, M. A.; Clark, N. A. *Science* **2000**/**2001**, *288*, 2181.

(17) de Gennes, P. G. *The Physics of Liquid Crystals*; Oxford University Press: London, 1974.

(18) (a) Jákli, A.; Krüerke, D.; Sawade, H.; Heppke, G. *Phys. Rev. Lett.* **2001**, *86*, 5715−5718. (b) Rauch, S.; Bault, P.; Sawade, H.; Heppke, G.; Nair, G. G.; Jákli, A. *Phys. Rev. E* **2002**, *66*, 021706-(1-5).

(19) (a) Pleiner, H. *Proc. Freiburger Arbeitstagung Flüssigkristalle* **1999**, *28*, 16. (b) Brand, H. R.; Cladis, P. E.; Pleiner, H. *Int. J. Eng. Sci.* **2000**, *38*, 1099−1117. (c) Brand, H. R.; Cladis, P. E.; Pleiner, H. *Phys. Rev. Lett.* **2001**, *86*, 4974.

(20) Maginnity, P. M.; Eisenmann, J. L. *J. Am. Chem. Soc.* **1952**, *74*, 6119−6121.

(21) Hodges, A. M.; Winter, R. W.; Winner, S. W.; Preston, D.; Gard, G. L. *J. Fluorine Chem.* **2002**, *114*, 3−8.

(22) Winter, R. W.; Dodean, R.; Smith, J. A.; Anilkumar, R.; Burton, D. J.; Gard, G. L. *J. Fluorine Chem.* **2003**, *122*, 251−253.

(23) (a) Rao, N. V. S.; Potukuchi, D. M.; Pisipati, V. G. K. M. *Mol. Cryst. Liq. Cryst.* **1991**, *196*, 71. (b) Brisbin, D.; de Hoff, R.; Lockhart, T. E.; Johnson, D. L. *Phys. Rev. Lett.* **1979**, *43*, 1171−1174. (c) Doane, J. W.; Parker, R. S.; Cvikl, B.; Johnson, D. L.; Fishel, D. L. *Phys. Rev. Lett.* **1972**, *28*, 1694−1696.

(24) Meglio, C. D.; Rananavare, S. B.; Svenson, S.; Thompson, D. H. *Langmuir* **2000**, *16*, 128−133.

(25) Altomare, A.; Cascarano, G.; Giacovazzo, C.; Guagliardi, A.; Burla, M. C.; Polidori, G.; Camalli, N. *J. Appl. Crystallogr.* **1994**, *27*, 435−436.

(26) (a) *TeXsan Software for Single-Crystal Structure Analysis*, version 1.7; Molecular Structures Corp.: Woodland, TX, 1997. (b) *Molecule for MacIntosh*, version 1.3.5d6; Erlangen, Germany, http://www.ccc.uni-erlangen.de/molecule.

(27) Becke, A. D. *J. Chem. Phys.* **1993**, *98*, 5648.

(28) Lee, C.; Yang, W.; Parr, R. G. *Phys. Rev. B* **1988**, *37*, 785−789.

(29) Frisch, M. J.; Trucks, G. W.; Schlegel, H. B.; Scuseria, G. E.; Robb, M. A.; Cheeseman, J. R.; Zakrzewski, V. G.; Montgomery Jr., J. A.; Stratmann, R. E.; Burant, J. C.; Dapprich, S.; Millam, J. M.; Daniels, A. D.; Kudin, K. N.; Strain, M. C.; Farkas, O.; Tomasi, J.; Barone, V.; Cossi, M.; Cammi, R.; Mennucci, B.; Pomelli, C.; Adamo, C.; Clifford, S.; Ochterski, J.; Petersson, G. A.; Ayala, P. Y.; Cui, Q.; Morokuma, K.; Malick, D. K.; Rabuck, A. D.; Raghavachari, K.; Foresman, J. B.; Cioslowski, J.; Ortiz, J. V.; Baboul, A. G.; Stefanov, B. B.; Liu, G.; Liashenko, A.; Piskorz, P.; Komaromi, I.; Gomperts, R.; Martin, R. L.; Fox, D. J.; Keith, T.; Al-Laham, M. A.; Peng, C. Y.; Nanayakkara, A.; Gonzalez, C.; Challacombe, M.; Gill, P. M. W.; Johnson, B. G.; Chen, W.; Wong, M. W.; Andres, J. L.; Head-Gordon, M.; Replogle, E. S.; Pople, J. A. *Gaussian 98*, revision A.9; Gaussian, Inc.: Pittsburgh, PA, 1998.

(30) Rananavare, S. B.; Pisipati, V. G. K. M.; Freed, J. H. *Liq. Cryst.* **1988**, *3*, 957−976.

(31) Pisipati, V. G. K. M.; Rananavare, S. B.; Freed, J. H. *Mol. Cryst. Liq. Cryst. Lett.* **1987**, *4*, 181.

(32) Potukuchi, D. M.; Rao, N. V. S.; Pisipati, V. G. K. M. *J. Mol. Liq.* **1990**, *50*, 1−12.

(33) Gray, G. W.; Goodby, J. W. G. *Smectic Liquid Crystals, Textures and Structures*; Leonard Hill: Glasgow, England, 1984.

(34) (a) Zannoni, C. *J. Mater. Chem.* **2001**, *11*, 2637−2646. (b) Jeffery, C. A.; Austin, P. H. *J. Geophys. Res.* **1997**, *102*, 25269−25283.

(35) For recent review see for example: (a) Iannacchione, G. S.; Park, S.; Garland, C. W.; Birgeneau, R. J.; Leheney, R. L. *Phys. Rev. E* **2002**, *67*, 011709-(1-13). (b) Garland, C. W.; Nounesis, G. *Phys. Rev. E* **1994**, *49*, 2964−2971.

(36) Sied, M. B.; Salud, J.; López, D. O.; Barrio, M.; Tamarit, J. L. *Phys. Chem. Chem. Phys.* **2002**, *4*, 2587−2593.

(37) (a) Dippel, M.; Maier, A.; Gimple, V.; Wider, H.; Evenson, W. E.; Rasera, R. L.; Schatz, G. *Phys. Rev. Lett.* **2001**, *87*, 95505-(1-4). (b) Wronski, C. R. M. *Br. J. Appl. Phys.* **1967**, *18*, 1731−1737.

(38) Adamson, A.; Gust, A. *Physical Chemistry of Surfaces*, 6th ed.; John Wiley-Interscience: New York, 1997; p 331.

(39) (a) Kumar, P. A.; Swathi, P.; Pisipati, V. G. K. M *Z. Naturforsch. A* **2002**, *57*, 226−232. (b) Systematic Crystallization studies on these transitions would be valuable and are planned.

(40) Defay, R.; Prigogine, I.; Bellemans, A.; Everett, D. H. In *Surface Tension and Adsorption*; John Wiley: New York, 1966; Chapter 18.

(41) Viney, C.; Russel, T. P.; Depero, L. E.; Twieg, R. J. *Mol. Cryst. Liq. Cryst.* **1989**, *168*, 63−82.

(42) Viney, C.; Twieg, R. J.; Gordon, B. R.; Rabolt, J. F. *Mol. Cryst. Liq. Cryst.* **1991**, *198*, 285−289.